with the behavior of $[Pd(9N3)_2][PF_6]_2$ (9N3 = 1,4,7-triazacyclononane) in which the apical nitrogen atoms are oriented away from the axial coordination sites.[15]

In contrast to 9S3, the S donor atoms of TT[9]OB are not preorganized in the free ligand, as the solution and solid-state structures show an exodentate conformation for the S donor atoms.[1] In spite of this, the structure of $PdCl_2$(TT[9]OB) demonstrates that TT[9]OB is able to achieve facial coordination[16] at Pd(II) similar to that observed for 9S3.[11-15] The positioning of the S3 atom in the coordination sphere of $PdCl_2$(TT[9]OB) and the temperature dependence of the ^1H NMR spectra are consistent with a fluxional process in solution which would interconvert S1 and S3 coordination to Pd via a pivot of the ligand about the Pd-S2 bond.[17] This process is not possible for the complex $PdCl_2$(TT[9]MB) because the *m*-xylyl unit imparts an increased rigidity to the complex and does not allow for the close approach of S3 to the Pd atom. The $-SCH_2CH_2SCH_2CH_2S-$ linkage of TT[9]MB has been shown to adopt a "bracket structure" in the free ligand which resembles a right angle in projection.[1] This feature is characterized in the solid state by S-C-C-S torsional angles of approximately 180°, and this has been shown to persist in solution.[1,3] It is proposed that upon coordination to Pd(II) only one of the SCH_2CH_2S units is rearranged from this anti placement to the gauche placement required for a five-membered chelate ring. Another interesting feature of $PdCl_2$(TT[9]MB) is the ligand conformation, which allows for simultaneous positioning of S donor atoms in exodentate *and* endodentate positions. The uncoordinated exodentate S3 atom could be employed in subsequent coordination to other metals or for aggregation of the mononuclear complex. This feature of TT[9]MB is the focus of current work.

Acknowledgment. We thank the Natural Sciences and Engineering Research Council of Canada and the donors of the Petroleum Research Fund, administered by the American Chemical Society, for financial support of this research.

Registry No. $PdCl_2(PhCN)_2$, 114220-66-5; $PdCl_2$(TT[9]OB), 136822-80-5; $PdCl_2$(TT[9]MB), 136822-81-6.

Supplementary Material Available: Listings of crystallographic data collection parameters, positional parameters, thermal parameters, nonessential bond distances and angles, and hydrogen atom parameters (Tables S-I-S-IX) (5 pages); listings of observed and calculated structure factors (Tables S-X and S-XI) (26 pages). Ordering information is given on any current masthead page.

(15) Hunter, G.; McAuley, A.; Whitcombe, T. W. *Inorg. Chem.* **1988**, *27*, 2634-2639.
(16) We have recently found that TT[9]OB can enforce facial coordination and octahedral geometry at Ag(I) in the complex $[Ag(TT[9]OB)_2][ClO_4]$.
(17) For an example of similar fluxional behavior, see: Lui, S.; Lucas, C. R.; Newlands, M. J.; Charland, J. P. *Inorg. Chem.* **1990**, *29*, 4380-4385.

Contribution from the Departments of Chemistry, Iowa State University, Ames, Iowa 50011, and Wabash College, Crawfordsville, Indiana 47933, Isotope and Structural Chemistry Group (INC-4), Los Alamos National Laboratory, Los Alamos, New Mexico 87544, and Arthur Amos Noyes Laboratory,† California Institute of Technology, Pasadena, California 91125

Vibrational and Electronic Spectra of $[Pt_2(SO_4)_4]^{2-}$ Complexes

Robert A. Newman,[1a] Don S. Martin,*[1a] Richard F. Dallinger,*[1b] William H. Woodruff,[1c] Albert E. Stiegman,[1d] Chi-Ming Che,[1d] William P. Schaefer,[1d] Vincent M. Miskowski,*[1d] and Harry B. Gray*[1d]

Received May 8, 1991

The vibrational and electronic spectra of axially ligated sulfate-bridged binuclear platinum complexes ($[Pt_2(SO_4)_4L_2]^{n-}$: L = OH_2, DMSO, *n* = 2; L = Cl, Br, *n* = 4) have been studied. Raman spectra acquired with near-UV excitation show bands assigned to Pt-O(sulfate) stretching (300-350-cm^{-1} region) for all complexes, while bands assigned to Pt-Pt and Pt-L stretching are seen for complexes (L = Cl, Br) that display preresonance Raman scattering within intense near-UV absorption bands assigned to the $\sigma(L) \rightarrow \sigma^*(Pt_2)$ electronic transition. Weaker electronic absorptions are assigned as metal-metal $^1(\sigma \rightarrow \sigma^*)$ (near 220 nm for L = OH_2, Cl) and $d\pi \rightarrow d\sigma^*(Pt_2)$ (350-500 nm). Single-crystal polarized absorption spectra (L = OH_2, DMSO) show that the weak absorption system in the 350-500-nm region consists of three *z*-polarized (metal-metal axis) bands and an *x,y*-polarized band. The L = OH_2, Cl complexes show weak emission bands in the 695-750-nm region when excited at 77 K with near-UV light. These emission bands are similar to those observed for $[Pt_2(HPO_4)_4L_2]^{n-}$ (L = OH_2, *n* = 2; L = Cl, *n* = 4) complexes. The emission lifetimes for the sulfate-bridged complexes (450 ± 50 ns, L = OH_2; 290 ± 20 ns, L = Cl) are much shorter, and the emission intensities are much weaker, than the corresponding properties of the phosphate-bridged complexes.

Introduction

The structures and spectroscopic properties of d^7-d^7 complexes containing metal-metal single bonds have attracted much attention.[2-5] Extensive investigations of binuclear Pt(III) complexes have established that the relatively long Pt-Pt bond in bridging-pyrophosphite ($P_2O_5H_2^{2-}$) species is significantly perturbed by both axial and equatorial ligand interactions.[5-7] The effects of ligand variations on the vibrational and electronic spectra of $(Rh^{II})_2$ carboxylates[8] and $(Rh^{II})_2$ isocyanides[9] also have been studied in detail.

Binuclear Pt(III) complexes with bridging sulfate and phosphate ligands are of special interest because they possess relatively short Pt-Pt bonds;[10,11] indeed, a study of the electronic spectra of several phosphate-bridged species has already appeared.[12] We have now completed an extensive spectroscopic examination (absorption, emission, and vibrational spectra and single-crystal polarized electronic absorption spectra) of the sulfate-bridged compounds, and the results are reported herein.

† Contribution No. 8442.

(1) (a) Iowa State University. (b) Wabash College. (c) Los Alamos National Laboratory. (d) California Institute of Technology.
(2) Cotton, F. A.; Walton, R. A. *Multiple Bonds Between Metal Atoms*; Wiley: New York, 1982; pp 347-351.
(3) (a) Miskowski, V. M.; Gray, H. B. In *Understanding Molecular Properties*; Avery, J., Dahl, J. P., Eds.; Reidel Publishing Co.: Dordrecht, Holland, 1987; pp 1-16. (b) Lever, A. B. P. *Inorganic Electronic Spectroscopy*, 2nd ed.; Elsevier: Amsterdam, 1984.
(4) (a) Felthouse, T. R. *Prog. Inorg. Chem.* **1982**, *29*, 73-166. (b) Cotton, F. A.; Walton, R. A. *Struct. Bonding* **1985**, *62*, 1-49. (c) Dunbar, K. R. *J. Am. Chem. Soc.* **1988**, *110*, 8247-8249.
(5) Roundhill, D. M.; Gray, H. B.; Che, C.-M. *Acc. Chem. Res.* **1989**, *22*, 55-61.
(6) (a) Che, C.-M.; Mak, T. C. W.; Gray, H. B. *Inorg. Chem.* **1984**, *23*, 4386-4388. (b) Alexander, K. A.; Bryan, S. A.; Fronczek, F. R.; Fultz, W. C.; Rheingold, A. L.; Roundhill, D. M.; Stein, P.; Watkins, S. F. *Inorg. Chem.* **1985**, *24*, 2803-2808. (c) Che, C.-M.; Lee, W. M.; Mak, T. C. W.; Gray, H. B. *J. Am. Chem. Soc.* **1986**, *108*, 4446-4451.
(7) Che, C.-M.; Mak, T. C. W.; Miskowski, V. M.; Gray, H. B. *J. Am. Chem. Soc.* **1986**, *108*, 7840-7841.

0020-1669/91/1330-4647$02.50/0

Experimental Section

The compounds $K_2[Pt_2(SO_4)_4(OH_2)_2]$,[13] $K_2[Pt_2(SO_4)_4(DMSO)_2]$[10a] (DMSO = dimethyl sulfoxide), $K_2[Pt_2(SO_4)_4(NH_3)_2]$,[13] $K_4[Pt_2(SO_4)_4Cl_2]\cdot H_2O$,[13] and $Cs_4[Pt_2(SO_4)_4Br_2]$[13] were all prepared by literature methods. In the preparation of the halide adducts, it was crucial to equilibrate the aqueous $[Pt_2(SO_4)_4(OH_2)_2]^{2-}$ starting material with the appropriate hydrohalic acid ($\sim 10^{-2}$ M) for about 15 min at room temperature, prior to precipitation with excess alkali-metal halide to avoid contamination with aquo complexes.

Solution electronic spectra were measured in 1 N H_2SO_4(aq) in most cases. Spectra for the halide adducts were obtained either by adding lithium halide to such solutions and equilibrating for ≥15 min or by dissolving the isolated halide adducts and immediately recording the spectra. The spectra obtained for $[Pt_2(SO_4)_4Cl_2]^{4-}$ were independent of preparation route, so long as the halide concentration was high (≥0.5 M). NMR studies have shown that formation of the dihalo complexes is incomplete at lower concentrations.[14]

The spectra of $[Pt_2(SO_4)_4Br_2]^{4-}$ solutions were complicated by decomposition. Overnight storage of 1 N H_2SO_4(aq) solutions containing 0.5 M LiBr showed complete disproportionation of the $[Pt_2(SO_4)_4]^{2-}$ unit to $PtBr_6^{2-}$ and $PtBr_4^{2-}$. The spectrum presented in the text was recorded 15 min after adjusting a 1 N H_2SO_4(aq) solution of $[Pt_2(SO_4)_4(OH_2)_2]^{2-}$ to 0.5 M LiBr when the absorbance at 345 nm had reached a maximum; the absorbance slowly decreased thereafter. Since the absorbances[3b] at ~310 ($PtBr_6^{2-}$) and ~270 nm ($PtBr_4^{2-}$) slowly increased with time, the weak shoulders present in our spectrum at these wavelengths at 15 min may not be authentic, and some decomposition (≤20%) may have occurred. However, the spectrum obtained immediately after dissolution of $Cs_4[Pt_2(SO_4)_4Br_2]$ in 1 N H_2SO_4(aq) is very similar to that presented. Preparation of solutions on a vacuum line with rigorous exclusion of oxygen had no effect.

Emission spectra were recorded[15] using either 366- or 404.6-nm Hg excitation. Emission lifetimes were obtained[16] using 353-nm excitation (Quanta-Ray DCR-1 Nd-YAG laser, third harmonic).

Raman and infrared spectra were obtained as previously described.[8b] Raman measurements used 363.8-nm excitation (argon ion laser); samples were pressed into K_2SO_4 or KCl pellets and spun to minimize decomposition. Far-infrared spectra were obtained on petroleum jelly mulls held between polyethylene plates.

Single-Crystal Spectroscopy. Large crystals of $K_2[Pt_2(SO_4)_4(OH_2)_2]$ were grown by dissolving a small amount of $K_2(H_3O)[Pt_2(SO_4)_4(OH)(H_2O)]$[13a] in a minimum quantity of hot distilled water, which was then acidified by a small amount of 0.005 M H_2SO_4 and slowly evaporated. The product included a number of thin, fractured rhomboidal crystals. A crystal was mounted on a goniometer head for indexing on an X-ray diffractometer. The following cell parameters were obtained: $a:b:c$ = 7.458:7.539:7.621 Å; $\alpha:\beta:\gamma$ = 102.27:110.85:100.22°; space group = $P\bar{1}$; V = 375.9 Å^3. These parameters are in satisfactory agreement with the parameters[10d] in a complex X-ray structure determination of the compound, viz. $a:b:c$ = 7.453 (3):7.524 (3):7.593 (3) Å; $\alpha:\beta:\gamma$ = 102.01 (4):111.45 (3):99.80 (3)°; $P\bar{1}$ space group; V = 373.1 (9) Å^3. The faces of the thin crystals were identified in the diffractometer as $\bar{1}00$ faces, and the rhomboidal edges were determined to be along the b and c axes. Between crossed polarizers in white light the extinctions were not absolute, indicating a wavelength dependence. This, of course, is to be expected for a triclinic crystal. For light polarized along one extinction (LO), a thin crystal appeared pale yellow, while along the other extinction (HI), the color was a much darker yellow, indicative of higher absorption. The HI extinction appeared about 13° from the b axis for light incident on a $\bar{1}00$ face.

The thickness of one crystal was measured to be 15 μm by a calibrated scale in the eyepiece of a microscope. At 6 K, the HI absorbance at 22 200 cm^{-1} for this crystal was measured to be 0.96, which corresponds to an extinction coefficient (ϵ) of 145 cm^{-1} M^{-1}. The thicknesses of other crystals were determined by measuring their HI absorbances at 22 200 cm^{-1}.

Large crystals of $K_2[Pt_2(SO_4)_4(DMSO)_2]\cdot 4H_2O$ were grown as described by Cotton et al.[10a] Among these were commonly found some thin, fragile, diamond-shaped yellow plates that were suitable for spectroscopic measurements. These crystals showed sharp, wavelength-independent extinctions parallel to the diamond diagonals, with the associated transmitted colors of yellow and dark orange for the two extinctions. A typical crystal was mounted on a diffractometer, and its space group was determined to be $P2_1/n$, consistent with the previous report.[10a] The b axis proved to be parallel to the yellow extinction, while the a axis was rigorously perpendicular to the crystal face. The dark orange extinction will accordingly be referred to as the $\perp a,b$ direction. Crystal thicknesses were not measured in this study.

The single-crystal spectra of $K_2[Pt_2(SO_4)_4(OH_2)_2]$[17] and $K_2[Pt_2(SO_4)_4(DMSO)_2]\cdot 4H_2O$[15] were obtained by methods described previously.

Results and Discussion

Structural Comparisons. Structural studies of binuclear Pt(III) complexes bridged by sulfate or phosphate ligands have revealed Pt–Pt bond distances[10d] ranging from 2.461 Å ($K_2[Pt_2(SO_4)_4(OH_2)_2]$) to 2.529 Å ($[Et_4N]_2[Pt_2(H_2PO_4)_2(HPO_4)_2Cl_2]\cdot H_2O$). Metal–metal distances for sulfate and phosphate analogues are very similar,[10] and there is some evidence[10c] that the metal–metal distance is insensitive to the degree of protonation of the bridging ligand.

We compare the structural data for these Pt(III) sulfate- and phosphate-bridged species with the results for three other types of Pt compounds. The first comparison involves α-pyridonate-bridged platinum complexes,[18] which are of particular interest because they are among the most highly oxidized of an extensive class[19] of oligomeric mixed-valence $Pt^{II}_nPt^{III}_x$ compounds. The Pt(III) compound $[Pt_2(NH_3)_4(C_5H_4NO)_2Cl_2](NO_3)_2$ displays[19] a Pt–Pt distance of 2.568 Å, very similar to that of the phosphate complex noted above. The Pt–Cl distances for the phosphate and α-pyridonate compounds are also similar, 2.445 and 2.44 Å (average), respectively. This encourages us to assume that the Pt–Pt (2.582 Å) and Pt–Br (2.57 Å, average) distances[18] in $[Pt_2(NH_3)_4(C_5H_4NO)_2Br_2]^{2+}$ are likely to be good estimates for $[Pt_2(SO_4)_4Br_2]^{4-}$, which has not been structurally characterized.

A different conclusion arises from comparisons with a second series,[6,7] the binuclear Pt(III) complexes bridged by four pyrophosphite units. The compound $K_4[Pt_2(P_2O_5H_2)_4Cl_2]$ displays[20] Pt–Pt and Pt–Cl bond distances of 2.695 and 2.407 Å, respectively. The Pt–Pt distance is distinctly longer, by 0.166 and 0.127 Å, than the distances in the phosphate and α-pyridonate species. This does not necessarily indicate a weaker Pt–Pt interaction, because the bridging pyrophosphite is a π-acceptor ligand. This changes the nature of the metal–metal σ symmetry orbitals by mixing metal p and ligand π* character into orbitals that would be mainly d_{z^2} for hard bridging groups.[3a] As a result, the optimum metal–metal bonding distance is longer. This may be why the Pt–Cl distance in the pyrophosphite complex is only slightly shorter than that in the other compounds, whereas consideration of the trans effect

(8) (a) Miskowski, V. M.; Schaefer, W. P.; Sadeghi, B.; Santarsiero, B. D.; Gray, H. B. *Inorg. Chem.* **1984**, *23*, 1154–1162. (b) Miskowski, V. M.; Dallinger, R. F.; Christoph, G. G.; Morris, D. E.; Spies, G. H.; Woodruff, W. H. *Inorg. Chem.* **1987**, *26*, 2127–2132. (c) Clark, R. J. H.; Hempleman, A. J. *Inorg. Chem.* **1989**, *28*, 746–752. (d) Trexler, J. W., Jr.; Schreiner, A. F.; Cotton, F. A. *Inorg. Chem.* **1988**, *27*, 3265–3264.

(9) Miskowski, V. M.; Smith, T. P.; Loehr, T. M.; Gray, H. B. *J. Am. Chem. Soc.* **1985**, *107*, 7925–7934.

(10) (a) Cotton, F. A.; Falvello, L. R.; Han, S. *Inorg. Chem.* **1982**, *21*, 2889–2891. (b) Conder, H. L.; Cotton, F. A.; Falvello, L. R.; Han, S.; Walton, R. A. *Inorg. Chem.* **1983**, *22*, 1887–1891. (c) Cotton, F. A.; Han, S.; Conder, H. L.; Walton, R. A. *Inorg. Chim. Acta* **1983**, *72*, 191–193. (d) Bancroft, D. P.; Cotton, F. A.; Falvello, L. R.; Han, S.; Schwotzer, W. *Inorg. Chim. Acta* **1984**, *87*, 147–153.

(11) El-Mehdaw, R.; Fronzcek, F. R.; Roundhill, D. M. *Inorg. Chem.* **1986**, *25*, 1155–1159.

(12) Shin, Y.-K.; Miskowski, V. M.; Nocera, D. G. *Inorg. Chem.* **1990**, *29*, 2308–2313.

(13) (a) Orlova, V. S.; Muraveiskaya, G. S.; Evstaf'eva, O. N. *Russ. J. Inorg. Chem. (Engl. Transl.)* **1975**, *20*, 753–758. (b) Muraveiskaya, G. S.; Kukina, G. A.; Orlova, V. S.; Evstaf'eva, O. N.; Porai-Koshits, M. A. *Dokl. Akad. Nauk SSSR* **1976**, *226*, 596–599. (c) Muraveiskaya, G. S.; Abashkin, V. E.; Evstaf'eva, O. N.; Golovaneva, I. F.; Schoelokov, R. N. *Koord. Khim.* **1980**, *6*, 463–472.

(14) Appleton, T. G.; Hall, J. R.; Neale, D. W. *Inorg. Chim. Acta* **1985**, *104*, 19–31.

(15) Rice, S. F.; Gray, H. B. *J. Am. Chem. Soc.* **1983**, *105*, 4571–4575.

(16) Nocera, D. G.; Winkler, J. R.; Yocom, K. M.; Bordignon, E.; Gray, H. B. *J. Am. Chem. Soc.* **1984**, *106*, 5145–5150.

(17) Fanwick, P. E.; Martin, D. S.; Webb, T. R.; Robbins, G. A.; Newman, R. A. *Inorg. Chem.* **1978**, *17*, 2723–2727.

(18) Hollis, L. S.; Robert, M. M.; Lippard, S. J. *Inorg. Chem.* **1983**, *22*, 3637–3644.

(19) Ginsberg, A. P.; O'Halloran, T. V.; Fanwick, P. E.; Hollis, L. S.; Lippard, S. J. *J. Am. Chem. Soc.* **1984**, *106*, 5430–5439 and references cited therein.

(20) Che, C.-M.; Herbstein, F. H.; Schaefer, W. P.; Marsh, R. E.; Gray, H. B. *J. Am. Chem. Soc.* **1983**, *105*, 4604–4607.

Table I. Calculated Force Constants (mdyn/Å) and Vibrational Frequencies (cm^{-1}) for $[Pt_2(SO_4)_4L_2]$ Complexes[a]

axial ligand	Pt–O(sulfate)		Pt_2		Pt–L_{ax}	
	k	ν	k	ν	k	ν
OH_2	3.14	333	2.52	200	2.13	468
Cl	3.14	333	2.19	179	1.95	332
Br	3.14	333	2.14	162	1.63	221

[a] Reference 23.

(competition for σ-bonding) might have led us to expect a large Pt–Cl shortening (toward a "normal" Pt–Cl distance of ~2.3 Å) when there is a large increase of the Pt–Pt distance. The structure of $[Pt_2(P_2O_5H_2)_4Br_2]^{4-}$ is strictly analogous to that of the dichloro complex.[6b] The Pt–Pt distance is 0.124 Å longer than that in the α-pyridonate analogue, but the Pt–Br distance (2.572 Å) is the same.

A final comparison is to the extensively studied series of axial adducts of the $[Rh_2(O_2CCH_3)_4]$ unit. The $[Rh_2(O_2CCH_3)_4Cl_2]^{2-}$ anion displays[8a] Rh–Rh and Rh–Cl distances of respectively 2.397 and 2.601 Å, while $[Rh_2(O_2CCH_3)_4(OH_2)_2]$ has[21] Rh–Rh and Rh–OH_2 equal to 2.3855 and 2.310 Å, respectively. Inasmuch as comparisons between second- and third-transition-series homologues usually show the latter to have longer (by ~0.1 Å) metal–metal bond distances,[2] the metal–metal bonding for the rhodium carboxylates would appear to be essentially equivalent to the $(Pt^{III})_2$ systems. The distinctly shorter axial metal–ligand bonds for the $(Pt^{III})_2$ compounds (metal–ligand bond distances for second- and third-transition-series homologues are usually very similar) probably reflect the higher formal charge on Pt(III) versus Rh(II), making the former less polarizable. The total charge of the binuclear unit does not affect the axial metal–ligand bond distances in the various Pt(III) series. Total charge also has no effect on the Rh(II) bridging complexes, as demonstrated by the nearly identical Rh–Rh and Rh–L bond distances for the axial OH_2 and Cl adducts of the $[Rh_2(CO_3)_4^{4-}]$[22] and $[Rh_2(O_2CCH_3)_4]$ units.

Vibrational Spectra. Vibrational spectra are reported for the $[Pt_2(SO_4)_4L_2]^{n-}$ complexes with axial ligands L = OH_2, Cl, Br. Vibrational data for the complexes with L = DMSO, NH_3 proved difficult to analyze due to complications from internal axial-ligand modes. We do note, however, that the far-infrared spectra of the aquo and ammine adducts are virtually identical in the 50–400-cm^{-1} range.

Our goal is to assign the core vibrational frequencies of the $[Pt_2O_8L_2]$ unit. We will first estimate these frequencies using[8b,23a] an empirical diatomic force constant–bond length relationship that depends only on the periodic table row number of each of the bonded partners.[23b] This relationship works quite well (estimated standard deviation ≈5%) for a wide variety of molecules in all physical states.

The results of our calculations are presented in Table I. The platinum–oxygen force constant was calculated[23b] using a Pt–O(sulfate) bond distance of 2.00 Å.[10d] The Pt–O frequency of 333 cm^{-1} was determined by assuming that the reduced mass for Pt–sulfate stretching is equal to half of the sulfate mass (a reasonable approximation for the symmetric mode and 90° O–Pt–Pt angles). This estimated Pt–O frequency is similar to those of the metal–oxygen modes in carboxylate-bridged binuclear metal complexes, which appear in the 300–380-cm^{-1} region.[24a]

The Pt–Pt and Pt–L (L = OH_2, Cl) force constants were calculated[23b] using published bond distances[10d] (for L = OH_2, r_{PtPt} = 2.461 Å and r_{PtL} = 2.111 Å from $K_2[Pt_2(SO_4)_4(OH_2)_2]$; for L = Cl, r_{PtPt} = 2.529 Å and r_{PtL} = 2.448 Å from $[Et_4N]_2[Pt_2(H_2PO_4)_2(HPO_4)_2Cl_2]$). The Pt–L diatomic frequencies were calculated using the simple Pt–L reduced masses, while the reduced masses used to determine the Pt–Pt frequencies were assumed to arise from the (LPt)–(PtL) "diatomic" unit. The estimated Pt–Pt frequencies for the two complexes vary due to changes in the force constant and the mass of the axial ligand.

The Pt–Pt and Pt–Br distances for the $[Pt_2(SO_4)_4Br_2]^{4-}$ complex were estimated from the $[Pt_2(NH_3)_4(C_5H_4NO)_2Br_2]^{2+}$ structure discussed in the previous section. The Pt–Br distance (2.57 Å) was taken directly from this structure, while the Pt–Pt distance was estimated to be 2.54 Å by assuming that the difference in the Pt–Pt distances for the Cl and Br adducts of the sulfate complexes is equal to the corresponding difference in the α-pyridonate-bridged complexes. The Pt–Pt stretching force constant and frequency for $[Pt_2(SO_4)_4Br_2]^{4-}$ were calculated in the same way as for the L = OH_2, Cl complexes.[24c] The estimated Pt–Br frequency is similar to the observed 224-cm^{-1} Pt–Br Raman frequency of $[Pt_2(P_2O_5H_2)_4Br_2]^{4-}$.[6b]

The Raman spectra of $K_2[Pt_2(SO_4)_4(OH_2)_2]$, $K_4[Pt_2(SO_4)_4Cl_2]$, and $Cs_4[Pt_2(SO_4)_4Br_2]$ are shown in Figure 1. Near-ultraviolet (363.8 nm) laser excitation was used with the aim of accessing preresonance intensity enhancement mechanisms within the intense UV metal–metal absorption bands (see Figure 2 for solution UV spectra). The electronic absorption spectra (vide infra) show that the 363.8-nm laser line is far from resonance for L = OH_2, but preresonant for L = Cl and near-resonant for L = Br. The Raman spectra show significant intensity enhancements along this series, as may be qualitatively gauged by comparing the intensity of the Raman lines relative to the Rayleigh scattering background at 100 cm^{-1}. These Raman data, along with the low-frequency infrared absorption data, are presented in Table II. The compounds show many intense lines above 400 cm^{-1}, particularly in

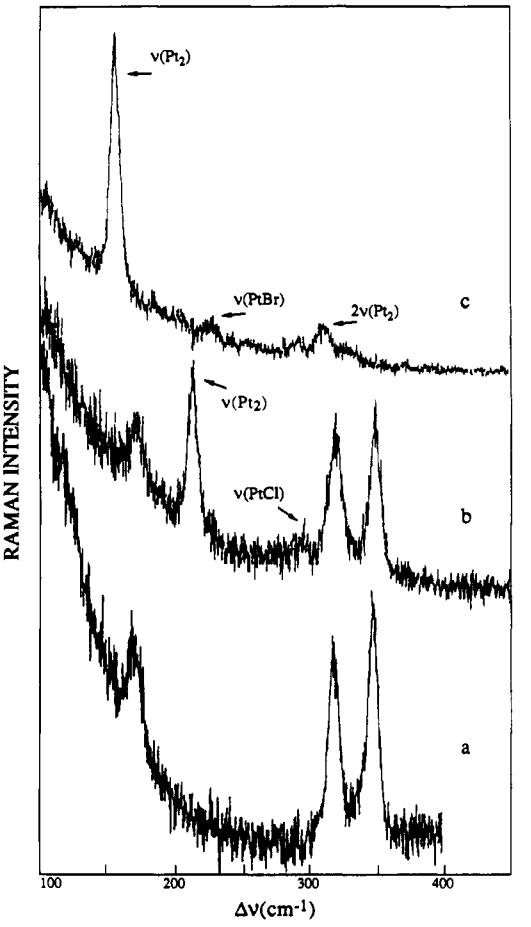

Figure 1. Raman spectra (363.8-nm excitation) of (a) $K_2[Pt_2(SO_4)_4(OH_2)_2]$ and spinning KCl pellets of (b) $K_4[Pt_2(SO_4)_4Cl_2]$ and (c) $Cs_4[Pt_2(SO_4)_4Br_2]$ (laser power ~10 mW at the sample; spectrometer slit width ~5.5 cm^{-1}).

(21) Cotton, F. A.; DeBoer, B. G.; LaPrade, M. D.; Pipal, J. R.; Ucko, D. A. *Acta Crystallogr., Sect. B.* **1971**, *B27*, 1664.
(22) Cotton, F. A.; Felthouse, T. R. *Inorg. Chem.* **1980**, *19*, 320–323.
(23) (a) Woodruff, W. H. Unpublished results. (b) Equations in: Conradson, S. D.; Sattelberger, A. P.; Woodruff, W. H. *J. Am. Chem. Soc.* **1988**, *110*, 1309–1311.
(24) (a) Miskowski, V. M.; Loehr, T. M.; Gray, H. B. *Inorg. Chem.* **1987**, *26*, 1098–1108. (b) Lowenschuss, A.; Shamir, J.; Ardon, M. *Inorg. Chem.* **1976**, *15*, 238–241. (c) Hopkins, M. D.; Miskowski, V. M.; Gray, H. B. *J. Am. Chem. Soc.* **1986**, *108*, 959–963.

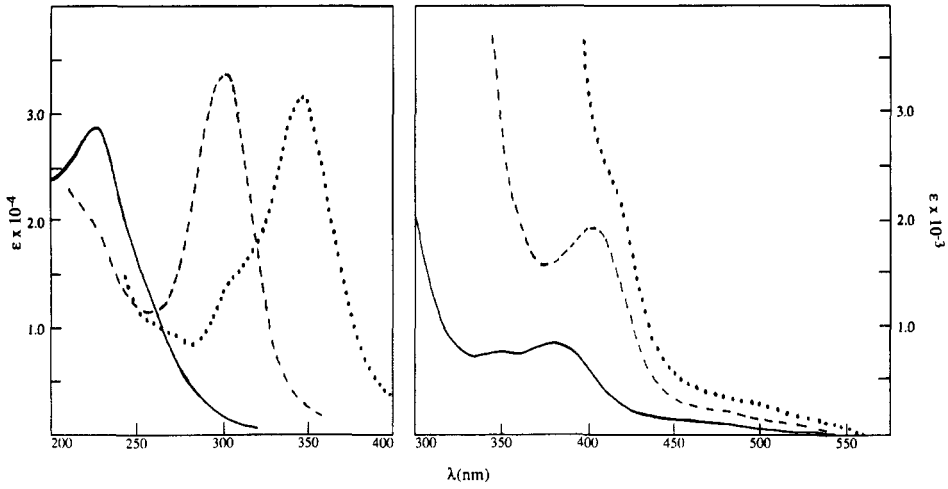

Figure 2. Electronic spectra of $[Pt_2(SO_4)_4L_2]^{4-}$ complexes in 1 N H_2SO_4(aq) solution at room temperature: —, L = OH_2; ---, L = Cl (0.6 M LiCl); ···, L = Br (0.5 M LiBr).

Table II. Observed Vibrational Frequencies (cm^{-1}) for Axial-Ligand Adducts of $[Pt_2(SO_4)_4]^{2-}$

	IR			Raman		
assgnt	OH_2	Cl	Br	OH_2	Cl	Br
				345	350	330
ν(Pt–O(sulfate))	320	320	313			311[b]
				318	320	293
ν(Pt–L)	*a*	(320)	237	...	296	228
$\nu(Pt_2)$					214	157
δ(Pt–O(sulfate))	202	203	207	170	173	
	155 sh	152 sh	189			
			150			
	90	90	109			

[a] Not assigned. [b] Assigned as the overtone $2\nu(Pt_2)$.

the IR spectra. These features, which are very similar to lines exhibited by sulfate-bridged binuclear molybdenum compounds,[24b,c] are mostly due to sulfate modes and will not be considered further.

The Raman spectrum of the diaquo complex (Figure 1a) shows three low-frequency (<400 cm^{-1}) lines (348, 318, and 170 cm^{-1}). The 348- and 318-cm^{-1} bands can be confidently assigned to ν(Pt–O(sulfate)) modes. The intensities of these bands (presumably one is associated with a symmetric mode and the other with a non totally symmetric, but gerade, mode) are consistent with the Raman data for $[Rh_2(O_2CCH_3)_4]$ complexes.[8b] The 170-cm^{-1} line is assigned to a Pt–O deformation mode, again by analogy to the $[Rh_2(O_2CCH_3)_4]$ spectra. The absence of a $\nu(Pt_2)$ band is consistent with the similar absence of perceptible intensity of $\nu(Rh_2)$ using near-UV excitation[8b] for $[Rh_2(O_2CCH_3)_4(OH_2)_2]$. As will be shown below, the UV spectra of Rh(II) and Pt(III) compounds are very similar, and $\nu(M_2)$ for the aquo complex is not enhanced by nearby electronic transitions in either case.

Our assignments for the aquo adduct are strengthened by the spectrum of the dichloro complex, which shows three lines at nearly the same frequencies (as the aquo). The dichloro complex shows two additional lines, presumably arising from preresonance enhancement within the intense 298-nm (vide infra) absorption. These bands, at 214 (strong) and 296 cm^{-1} (weak), are respectively assigned to $\nu(Pt_2)$ and ν(Pt–Cl) on the basis of both intensity arguments (the metal–metal stretch is expected to be strongly enhanced for excitation in a metal–metal-axis-localized transition) and frequency estimates (Table I).

The Raman spectrum of the dibromo adduct is quite different from that of the other compounds. Resonance effects yield intense scattering, and the spectrum is dominated by a strong band at 157 cm^{-1}. From the frequency estimates (Table I) we suggest an assignment of $\nu(Pt_2)$ for this line. A weak feature at 228 cm^{-1} is assigned to a_{1g} ν(Pt–Br). In the cluster of three weak lines near 300 cm^{-1}, the 293- and 330-cm^{-1} features are attributed to ν(Pt–O(sulfate)) by analogy to the other complexes; and the 311-cm^{-1} line, which is the strongest band in the cluster, is assigned to the overtone of the metal–metal stretch, $2\nu(Pt_2)$. Attempts to observe higher overtones were complicated by photodecomposition upon prolonged exposure of the sample pellet to UV laser excitation.

Appleton et al.[14] have reported aqueous solution Raman data (514.5-nm excitation) for a number of axial adducts (L = OH_2, OH, Cl, Br, NO_2, CN, NH_3) of $[Pt_2(SO_4)_4]^{2-}$ and $[Pt_2(HPO_4)_4]^{2-}$. Most of these compounds exhibit a line at 210–236 cm^{-1} attributed to $\nu(Pt_2)$, and our present work indicates that this assignment is reasonable. Aquo adducts show lines near 300 cm^{-1} that were also assigned to $\nu(Pt_2)$; our analysis indicates that these lines should be reassigned to ν(Pt–O). Bands reported at 320–340 cm^{-1} for chloride adducts were assigned to ν(Pt–Cl). These assignments are reasonable, but ν(Pt–O) assignments are also possible. The spectrum reported by Appleton et al.[14] for $[Pt_2(SO_4)_4Br_2]^{4-}$ exhibits two lines (210 and 193 cm^{-1}) that were not present in our spectra. Since we have found this ion to be rather unstable in solution, we suggest that decomposition may have occurred under the conditions of Appleton's experiment.[14] We note that $PtBr_6^{2-}$ and $PtBr_4^{2-}$ (two decomposition products we have observed) have a_{1g} Raman lines at 213 and 208 cm^{-1}, respectively.[25] We also note that Mahtani and Stein have recently reported $\nu(Pt_2)$ to be in the range 170–184 cm^{-1} for α-pyridonate-bridged Pt(III) compounds,[26] which is consistent with our results.

The far-infrared spectra of the three complexes (L = OH_2, Cl, Br) studied in detail show two intense, broad features below 400 cm^{-1} (~320 and ~200 cm^{-1}; see Table II). They are attributable to Pt–O(sulfate) stretching and deformation modes, respectively. Weak features below 200 cm^{-1} are probably also associated with deformation modes.

The IR spectrum of $Cs_4[Pt_2(SO_4)_4Br_2]$ additionally shows an intense line at 237 cm^{-1}, which we assign to a_{2u} ν(Pt–Br) (although it is far from certain that the assignments of the 237- and 207-cm^{-1} features might not be reversed). No features that could be attributed to axial ligand stretching modes emerged from the far-infrared spectra of the other two compounds. The spectrum of the diaquo adduct does show a broad band at 425 cm^{-1}, near the Table I prediction for ν(Pt–OH_2), but the spectra of the other compounds all show similar features, indicating that this band is a sulfate mode.[24b] Presumably, the sulfate band intensity obscures ν(Pt–OH_2). The best explanation for the absence of ν(Pt–Cl) is that the broad, intense ν(Pt–O(sulfate)) band obscures it. We also note that the band assigned[6b] as ν(Pt–Cl) in the infrared spectrum of $K_4[Pt_2(P_2O_5H_2)_4Cl_2]$ is not very intense.

Electronic Spectra. Electronic spectra were recorded in acidic solution, typically 1 N H_2SO_4(aq), to suppress the protona-

(25) Nakamoto, K. *Infrared and Raman Spectra of Inorganic and Coordination Compounds*, 4th ed.; Wiley-Interscience: New York, 1986.
(26) Mahtani, H. K.; Stein, P. *J. Am. Chem. Soc.* **1989**, *111*, 1505–1506.

Table III. Electronic Absorption Data at Room Temperature for $[Pt_2(SO_4)_4L_2]^{n-}$ Complexes in 1 N H_2SO_4(aq)[a]

L	band I	II	III	IV	V	VI
OH_2	465 (150 sh)	380 (900)	348 (770)	260 (1200 sh)		224 (28 700)
Cl^b	480 (300 sh)	401 (1850)			298 (33 500)	220 (20 000 sh)
$Br^{b,c}$	500 (400 sh)	420 (2200 sh)			345 (31 100)	

[a] Entries given as λ_{max} (nm) (ϵ_{max}). Vacant entries not observed or obscured by anion absorption. [b] Solution is 0.5 M in lithium halide. [c] See Experimental Section.

tion/deprotonation equilibria of the ligands.[13] Both solubility and stability are significantly higher in acidic solution. However, we found no changes in the band positions for acid concentrations ranging from 2 to 10^{-4} M, and moreover, spectra recorded in 0.1 M aqueous H_2SO_4, $HClO_4$, and CF_3SO_3H were all the same. For acidic solutions less than 10^{-4} M, axial-water deprotonation,[13] with concomitant spectral changes, appears to occur. In the more acidic regime, it is conceivable that there are variations in the degree of protonation of the bridging sulfate ligands.[10] If so, the electronic structure of the $(Pt^{III})_2$ unit is insensitive to such protonation. The ^{195}Pt NMR spectra also have been reported[14] to be insensitive to pH in acidic solutions.

Absorption spectra of the aquo, chloro, and bromo adducts of $[Pt_2(SO_4)_4]^{2-}$ are shown in Figure 2 (the data are summarized in Table III). The intense bands (designated V) of the chloro and bromo complexes at 298 and 345 nm, respectively, are readily assigned to axial-ligand-to-metal charge transfer (LMCT), $\sigma(X) \rightarrow \sigma^*(Pt_2)$, because of the pronounced axial-ligand sensitivity. The spectra of the phosphate analogues[12] are nearly identical with our sulfate spectra, and a similar axial-ligand sensitivity for pyrophosphite-bridged complexes has been noted.[5,6]

The aquo complex exhibits intense absorption at 224 nm (band VI), while the chloro derivative has a shoulder at 220 nm. Similar features have been seen for $[Rh_2(O_2CCH_3)_4]$ valence-isoelectronic analogues,[8a] as well as for Pt(III) binuclear complexes with bridging phosphate[12] and pyrophosphite[7] ligands. The most likely assignment to the metal–metal $^1(\sigma \rightarrow \sigma^*)$ transition, consistent with previous work.[7,8a,b] An alternative assignment is to an equatorial charge-transfer transition, e.g., sulfate-to-platinum CT. The persistence of the band at similar wavelengths for the several types of compounds listed above argues against this interpretation, however. The shoulder at 260 nm in the spectrum of the aquo complex (band IV), which is not resolved for the other compounds, could be due to an equatorial LMCT ($SO_4^{2-} \rightarrow$ Pt(III)) transition.

There are additional weak absorption bands in the 300–600-nm region (bands I–III of Table III). Band III is only resolved for the aquo adduct at room temperature. At 5 K, a CsCl pellet of $K_4[Pt_2(SO_4)_4Cl_2]$ exhibits band III as a shoulder at ~360 nm; similar resolution of an analogous feature has been noted previously[12] for glassy solutions of $[Pt_2(HPO_4)_4Cl_2]^{4-}$ at 77 K. Unfortunately, none of the absorption bands of $K_4[Pt_2(SO_4)_4Cl_2]$ (in CsCl) or $K_2[Pt_2(SO_4)_4(OH_2)_2]$ (in K_2SO_4) shows any vibronic structure at 5 K.

There are two possible assignments for bands I–III. First, they might be ligand-field (LF) transitions of the type $d\pi(\pi/\pi^*, \delta/\delta^*)$ to $d_{x^2-y^2}\sigma^*(Pt-O)$. The electronic spectrum of the $[Pt(OH_2)_4]^{2+}$ ion has been reported,[27] and the lowest energy resolved d–d transitions are at (assignments[27] in parentheses) 273 (ϵ = 56.5, $^1(d_{xz,yz} \rightarrow d_{x^2-y^2})$), 320 ($\epsilon$ = 15, $^1(d_{xy} \rightarrow d_{x^2-y^2})$), and 390 nm ($\epsilon$ = 10, singlet → triplet). Because metal–metal interactions[2] should lower the energies of transitions[28] from filled antibonding metal–metal orbitals (π^*, δ^*), LF bands might lie in the 300–600-nm region for the binuclear Pt(III) species. The intensities observed for bands I and II do seem rather high for such an assignment, however, as compared to the mononuclear analogue.

An alternative possibility is transitions of the type $d\pi(\delta/\delta^*, \pi/\pi^*) \rightarrow d\sigma^*(Pt_2)$. A strong argument in favor of this assignment is that bands of similar intensities and wavelengths have been reported for the $[Pt_2(P_2O_5H_2)_4(NCCH_3)_2]^{2-}$ ion[7] and related halide adducts.[6] The high LF strength[28] of $P_2O_5H_2^{2-}$ makes an LF assignment extremely unlikely for the latter complexes.

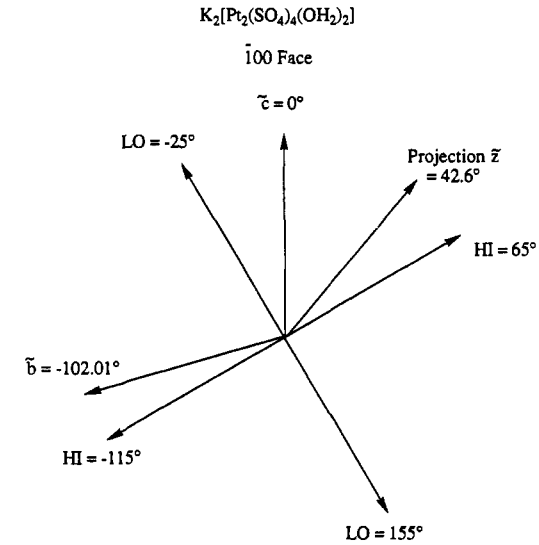

Figure 3. Arrangements of the crystallographic axes, optical extinctions, and projection of the molecular z axis on the spectroscopic face (1̄00) for $K_2[Pt_2(SO_4)_4(OH_2)_2]$.

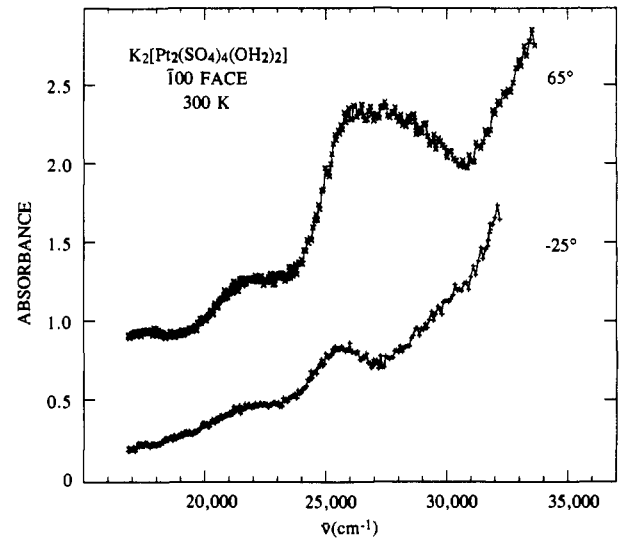

Figure 4. Spectra at 300 K of a 9.1 μm thick crystal of $K_2[Pt_2(SO_4)_4(OH_2)_2]$ for the HI and LO polarized angles.

Single-Crystal Spectra. $K_2[Pt_2(SO_4)_4(OH_2)_2]$. The local symmetry about the metal–metal (z) axis in $[Pt_2(SO_4)_4(OH_2)_2]^{2-}$ is very nearly D_{4h}. The projection of the z axis upon the 1̄00 face of the crystal is 42.6° from the c axis or 22.4° from the HI extinction (Figure 3). Therefore, a z-polarized transition should be more intense along the HI extinction than the LO with an expected polarization intensity ratio, HI/LO = $\cos^2 22.4°/\cos^2 67.6°$ = 5.89.

Single-crystal absorption spectra along the HI and LO extinctions at 300 K are shown in Figure 4. To check the possibility of wavelength dependence of the crystal transition moment, spectra at 6 K were recorded in 10° steps of polarization angle in the

(27) Elding, L. I. *Inorg. Chim. Acta* **1976**, *20*, 65–69.
(28) Stiegman, A. E.; Rice, S. F.; Gray, H. B.; Miskowski, V. M. *Inorg. Chem.* **1987**, *26*, 1112–1116.

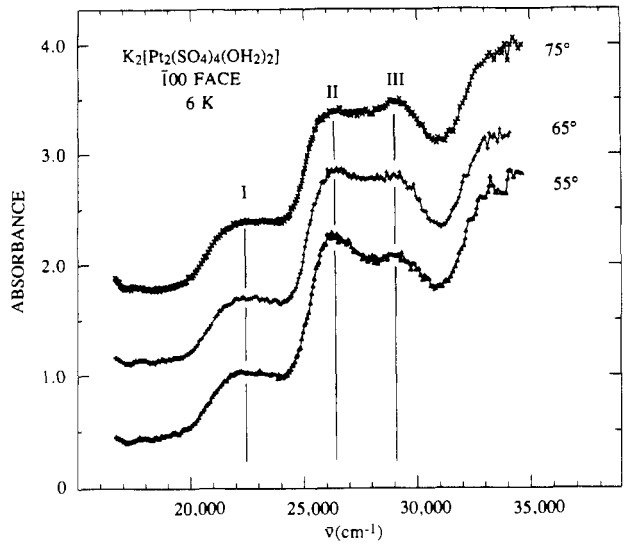

Figure 5. Spectra at 6 K of a 9.1 μm thick crystal of $K_2[Pt_2(SO_4)_4(OH_2)_2]$ with polarizer angles in the vicinity of the HI extinction angle (65°).

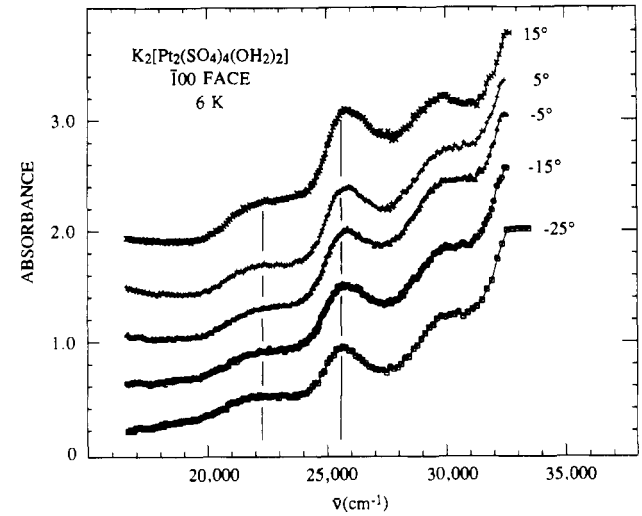

Figure 6. Spectra at 6 K of a 9.1 μm thick crystal of $K_2[Pt_2(SO_4)_4(OH_2)_2]$ with polarizer angles in the vicinity of the LO extinction (−25°).

vicinity of the HI (Figure 5) and LO (Figure 6) polarizations. The low-temperature spectra show considerably better resolution and slightly higher intensities than the 300 K spectra. The fact that the intensities do not decrease at low temperatures indicates that these are electric-dipole-allowed rather than vibronically excited transitions. In the 6 K spectrum at 65° (Figure 5), three broad components (with maxima at 22 400, 26 300, and 29 100 cm^{-1}) are clearly seen. The change in band shapes indicates significant wavelength dependence of the extinction polarization. The absorbances at 22 400 and 29 100 cm^{-1} (measured as the differences from the absorbance at 18 000 cm^{-1}) are nearly the same for polarizations of 55, 65, and 75°, consistent with the extinction direction of approximately 65° observed with the crossed polarizers. However, there is a definite increase in intensity at 26 300 cm^{-1} from the 75 to the 65 to the 55° polarization, thereby indicating that the extinction direction is probably somewhat lower than 55°. Thus, this peak is the most intense feature at 55° (it is somewhat weaker than the 29 100-cm^{-1} component at 75°). The 22 400- and 29 100 cm^{-1} components can be seen in the LO polarizations, where their intensities are consistent with the polarization ratio (5.9) predicted for a *z*-polarized transition.

There is a band maximum at 25 600 cm^{-1} in the −25° spectrum; this maximum is approximately 700 cm^{-1} lower than the most intense feature in the 55° spectrum. Furthermore, the magnitude of the −25° peak is 37% of the 55° peak. It is likely, therefore, that the 25 600-cm^{-1} peak represents an *x,y*-polarized transition.

Table IV. Single-Crystal Absorption Data for $K_2[Pt_2(SO_4)_4(OH_2)_2]$ at 6 K

band	λ, nm	ν, cm^{-1}	max pol, deg	ϵ_{max}
I	446	22 400	55 (*z*)	~145
IIa	391	25 600	−25 (*x,y*)	~180
IIb	380	26 300	55 (*z*)	~430
III	344	29 100	75 (*z*)	~410

Table V. Calculated Normalized Intensities for Dipole-Allowed Electronic Transitions of $K_2[Pt_2(SO_4)_4(DMSO)_2]\cdot 4H_2O$

	dipole moment			
	$\|\|b$	$\perp b,a$	$\|\|a$	$I(\perp a,b)/I(\|\|b)$
z	0.012	0.105	0.882	8.61
x,y	0.988	0.895	0.117	0.91

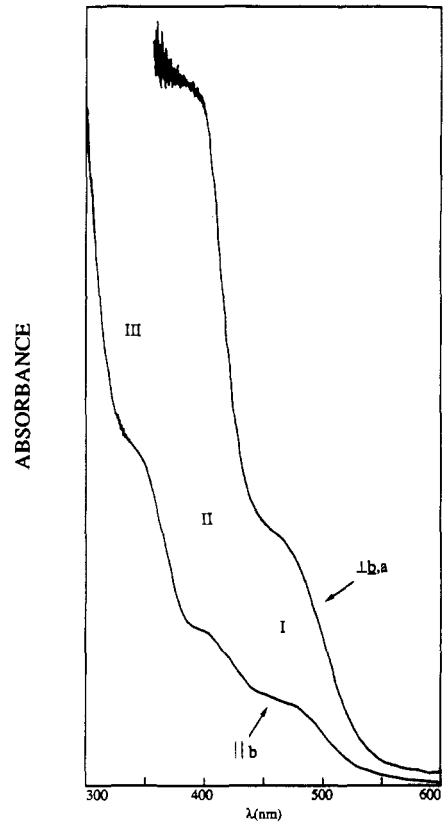

Figure 7. Spectra at 300 K of a crystal of $K_2[Pt_2(SO_4)_4(DMSO)_2]\cdot 4H_2O$ for the indicated polarizations. The $\perp b,a$ spectrum is vertically offset from the $\|b$ spectrum for clarity.

The experiments have revealed that there are three *z*-polarized bands and a weak *x,y*-polarized system in the I–III region of $[Pt_2(SO_4)_4(OH_2)_2]^{2-}$ (Table IV). The polarization assignments are predicted on the assumption that the molecular transition moment is aligned with the Pt–Pt bond. Since the site symmetry for the dimer is only $\bar{1}$ in the triclinic crystal, this assumption is open to question. In the case of the triclinic crystals[29] of binuclear $[Mo_2(O_2CCH_3)_4]$, for example, it was found from spectra for two different faces that the transition moment had shifted from the molecular axis sufficiently to invert the polarization ratios for a particular face. In that case, the shift appeared to be the result of asymmetry introduced by intermolecular bonding that involved O atoms bonded to the metal atoms. It does not seem likely that $[Pt_2(SO_4)_4(OH_2)_2]^{2-}$ would experience as great a perturbation.

$K_2[Pt_2(SO_4)_4(DMSO)_2]\cdot 4H_2O$. In an attempt to resolve some of the uncertainties resulting from the triclinic crystal structure of $K_2[Pt_2(SO_4)_4(OH_2)_2]$, we investigated an analogous compound

(29) Martin, D. S.; Newman, R. A.; Fanwick, P. E. *Inorg. Chem.* **1979**, *18*, 2511–2520.

having a higher symmetry lattice. The compound $K_2[Pt_2(SO_4)_4(DMSO)_2]\cdot 4H_2O$ (monoclinic $P2_1/n$ lattice)[10a] was selected for study since its O-bonded DMSO axial ligands should be closely analogous to OH_2 axial ligands. Thin crystal faces containing the crystallographically unique b axis were readily obtained (see Experimental Section). Calculated electric-dipole polarization ratios for the crystal face that was studied are given in Table V, and the room-temperature polarized spectra are shown in Figure 7.

Unfortunately, while similar room-temperature data were obtained for three different crystals, each of them developed cracks (and, hence, light leaks) upon cooling to 5 K for low-temperature measurements. Our low-temperature absorption data for the weak $\|b$ polarization were of sufficient quality to show that no new bands (as compared to room temperature) had appeared and that no vibronic structure had been resolved.

Inspection of Figure 7 reveals that bands I–III are all predominantly molecular z-polarized, consistent with our results for the diaquo complex. A peculiarity of the crystal face that was studied is that there is little contribution from molecular z polarization for any polarization angle. Thus, the molecular z axis must be nearly perpendicular to the crystal face. This explains why the $\|b$ spectrum in Figure 7 differs from those of the diaquo complex in an isotropic medium (Figure 2) and in single crystals (Figures 4–6). Specifically, we propose that an intense molecular x,y-polarized band to higher energy (possibly band IV of Table III) may contribute strongly to these spectra by providing a rising background that, due to the crystal orientation, is much stronger than that of the isotropic spectrum.[30]

The polarization ratios nonetheless eliminate x,y polarization for bands I–III. Observed values of $I(\perp b,a)/I(\|b)$ are 2.8 for band I and 4.5 for band II. Crystals sufficiently thin to observe band II in $\perp b,a$ polarization could not be obtained, but the intensity in $\|b$ polarization, assuming an isotropic intensity similar to that of Figure 2, indicates that band III also must be predominantly z-polarized.

The significance of the polarization ratio for band II being lower than the theoretical z-polarized value of 8.61 (Table V) is doubtful, particularly since the rising x,y-polarized absorption at higher energy may contribute significantly to the net intensity at the band II maximum. However, it is not inconsistent with our earlier conclusion that there is an x,y-polarized component of band II for the diaquo complex.

That the polarization ratio of band I is much less than that of band II is clearly significant, indicating that band I must contain an x,y-polarized absorption component. Because band I is poorly resolved from band II and other higher lying absorptions, it is difficult to quantify the x,y-polarized contribution.[31] The x,y contribution is observed by comparing the relative intensities of bands I and II in $\|b$ polarization (Figure 7) to those of other figures. Since the band shapes are similar in the two polarizations, the z- and x,y-polarized intensity components must be nearly coincident.

Electronic Emission Spectra. Polycrystalline samples of $K_2[Pt_2(SO_4)_4(OH_2)_2]$ and $K_4[Pt_2(SO_4)_4Cl_2]$ both show weak red electronic emission at 77 K when excited with UV or near-UV light (Figure 8). The emission maxima for axial-OH_2 (694 nm) and -Cl (755 nm) complexes are both similar to those recently reported[12] for the bridging phosphate analogues, but the emission intensities are much weaker. In addition, the emission lifetimes (355-nm excitation: 450 ± 50 ns, OH_2; 290 ± 20 ns, Cl) are considerably shorter at 77 K than those observed for the phosphate complexes under the same conditions (1.6 μs, $K_2[Pt_2(HPO_4)_4(OH_2)_2]$; 29 μs, $K_4[Pt_2(HPO_4)_4Cl_2]$). The emission of the sulfate complexes remains weak at temperatures down to 5 K, and no vibronic structure was resolved at any temperature.

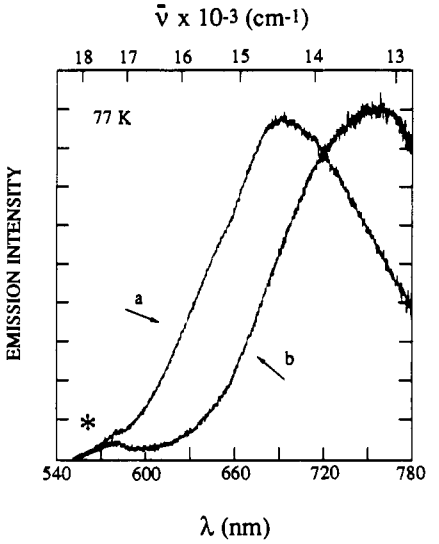

Figure 8. Emission spectra at 77 K of polycrystalline samples of (a) $K_2[Pt_2(SO_4)_4(OH_2)_2]$ and (b) $K_4[Pt_2(SO_4)_4Cl_2]$ with 404.6-nm Hg excitation. The weak feature indicated by an asterisk is due to a Hg emission line.

Emission could not be detected at room temperature from solid or solution samples. It appears that there is a strong temperature dependence of the emission (decreasing at high temperatures) analogous to that characterized for the phosphate analogues.[12] The emission intensity for the aquo complex drops to nearly zero at ~570 nm (Figure 8), and the absorption intensity is negligible near 530 nm (Figure 5). Thus, there is a gap of ~1300 cm^{-1} between absorption band I and the emission. Estimating the half-width of absorption band I to be about 3000 cm^{-1} (roughly equal to the half-width of the emission band, as seen in Figure 8), we calculate[32] a radiative rate constant k_r of 4×10^5 s^{-1} for emission from the excited state of band I for both sulfate and phosphate complexes.

In contrast, measurements of emission quantum yields and lifetimes suggest $k_r \sim 10^3$ s^{-1} for $[Pt_2(HPO_4)_4(OH_2)_2]^{2-}$ and $[Pt_2(HPO_4)_4Cl_2]^{4-}$.[12] This value is over 2 orders of magnitude smaller than our band I estimate, thereby indicating that the emissive excited state involves a transition that is more forbidden than the one associated with band I. This forbidden transition presumably lies in the gap between emission and absorption (a detailed discussion of this point is given by Shin et al.).[12]

Assignments of Bands I–III. The single-crystal absorption results indicate predominantly molecular z polarization for bands I–III. One possible explanation for this curious observation is that low-symmetry-induced coupling[8a] of $d\pi \rightarrow d\sigma^*$ transitions to the strongly allowed z-polarized $d\sigma \rightarrow d\sigma^*$ and/or axial LMCT transitions can result in stolen molecular z-polarized intensity. Moreover, the considerable increase in the intensities of bands I–III for the halide adducts (Table III) as the energy of axial LMCT (band IV) decreases is consistent with this intensity-stealing mechanism.

We assign bands II and III, respectively, to the metal–metal $^1(\pi^* \rightarrow \sigma^*)$ ($^1A_{1g} \rightarrow {}^1E_u$) and $^1(\delta^* \rightarrow \sigma^*)$ ($^1A_{1g} \rightarrow {}^1B_{2g}$) transitions. The x,y-polarized component IIa (Table IV) might reflect the intrinsic x,y-dipole-allowed character of $^1(\pi^* \rightarrow \sigma^*)$. We additionally suggest that band I be assigned to the $^3(\pi^* \rightarrow \sigma^*)$ ($^1A_{1g} \rightarrow {}^3E_u$) transition. The ^3E_u level is split by spin–orbit coupling (in the D_{4h}' double group) into five states (E_u, A_{1u}, A_{2u}, B_{2u}, and B_{2u} symmetries). Mixing of the E_u spin–orbit component with the ^1E_u state is expected to be the major mechanism for gaining singlet character, thereby accounting for the mixed polarization of band I.

(30) We have not determined the solution absorption spectrum of $K_2[Pt_2(SO_4)_4(DMSO)_2]$, because the only solvent in which it is appreciably soluble is water. The strong absorption of the added DMSO that would be necessary to give the $(DMSO)_2$ adduct in water would obscure the entire UV region.

(31) Curve resolution suggests a "corrected" $I(\perp b,a)/I(\|b)$ of ~1.5 for band I; from Table V we calculate an intensity ratio $I(z)/I(x,y) \approx 7$. This calculated value is extraordinarily sensitive to small errors, however.

(32) Strickler, S. J.; Berg, R. A. *J. Chem. Phys.* **1962**, *37*, 814–822.

Acknowledgment. Work performed at Iowa State University (R.A.N., D.S.M.) was supported by NSF Grants CHE76-83665 and CHE80-007441; we are indebted to Professor R. A. Jacobson, who provided the X-ray diffraction equipment. Research at the California Institute of Technology (A.E.S., C.-M.C., W.P.S., V.M.M., H.B.G.) was supported by the Office of Naval Research and the National Science Foundation. Portions of this work (R.F.D., W.H.W.) were performed at Los Alamos National Laboratory under the auspices of the U.S. Department of Energy.

Registry No. $K_2[Pt_2(SO_4)_4(OH_2)_2]$, 70085-58-4; $K_4[Pt_2(SO_4)_4Cl_2]$, 58807-44-6; $Cs_4[Pt_2(SO_4)_4Br_2]$, 60910-61-4; $K_2[Pt_2(SO_4)_4(DMSO)_2]\cdot 4H_2O$, 81602-75-7.

Contribution from the Department of Chemistry and Biochemistry, University of Notre Dame, Notre Dame, Indiana 46556

Spectroscopic and Electrochemical Characterization of Nickel β-Oxoporphyrins: Identification of Nickel(III) Oxidation Products

Patricia A. Connick and Kathleen A. Macor*

Received October 12, 1990

Seven nickel di- and tri-β-oxoporphyrins ([3,3,7,8,12,13,17,17-octaethyl-2,18(3*H*,17*H*)-porphinedionato(2-)]nickel, [3,3,8,8,12,13,17,18-octaethyl-2,7(3*H*,8*H*)-porphinedionato(2-)]nickel (NiDP-II), [3,3,7,7,12,13,17,18-octaethyl-2,8(3*H*,7*H*)-porphinedionato(2-)]nickel, [3,3,7,8,12,12,17,18-octaethyl-2,13(3*H*,12*H*)-porphinedionato(2-)]nickel, [3,3,7,8,13,13,17,18-octaethyl-2,12(3*H*,13*H*)-porphinedionato(2-)]nickel, [3,3,7,8,12,12,18,18-octaethyl-2,13,17(3*H*,12*H*,18*H*)-porphinetrionato(2-)]nickel (NiTP-A), and [3,3,8,8,13,13,17,18-octaethyl-2,7,12(3*H*,8*H*,13*H*)-porphinetrionato(2-)]nickel) were prepared by hydrogen peroxide oxidation of octaethylporphyrin followed by metalation. These compounds and the previously synthesized nickel mono-β-oxoporphyrin [3,3,7,8,12,13,17,18-octaethyl-2(3*H*)-porphinonato(2-)]nickel (NiMP) (Stolzenberg, A. M.; Glazer, P. A.; Foxman, B. M. *Inorg. Chem.* **1986**, *25*, 983-991) were characterized by electronic absorption spectroscopy, ^{1}H NMR spectroscopy, resonance Raman (RR) spectroscopy, and cyclic voltammetry. EPR spectra of the one-electron-oxidation products of NiMP, NiDP-II, and NiTP-A in methylene chloride and acetonitrile have also been obtained. A solvent-induced switch in the site of one-electron abstraction occurs in NiDP-II, where a Ni^{III}DP-II series is produced in acetonitrile solution and a Ni^{II}DP-II cation radical is generated in methylene chloride solution. In both solvents one-electron oxidation of NiMP yields a Ni^{II}MP cation radical while one-electron oxidation of NiTP-A yields Ni^{III}TP-A species. EPR signals from the Ni(III) centers (g_{av} = 2.24) are observed at liquid-nitrogen temperature. This is the first report of the Ni(III) state in a porphyrinic derivative at room temperature. The $Ni^{3+/2+}$ potential for NiTP-A is 0.34 V (vs SCE), which is one of the lowest reported for this redox couple. We suggest that stabilization of Ni(III) by the β-oxoporphyrins is based on a balance of π-conjugation, ring ruffling, and axial ligation. The nickel β-oxoporphyrins exhibit a greater number of Raman bands than nickel octaethylporphyrin (NiOEP) due to their lower symmetry. Vibrational modes that are only IR-active in NiOEP (D_{4h} symmetry) are observed with strong intensities in the Raman spectra of the nickel β-oxoporphyrins, which are best described as having C_2 symmetry. A carbonyl stretching mode in the 1708-1716-cm^{-1} region is observed as one of the strongest bands in the RR spectrum of each nickel β-oxoporphyrin, and is an identifying feature of the β-oxoporphyrin spectra.

Introduction

Nature uses a variety of porphyrinic ligands to bind metal ions in enzymes. Examples are the ubiquitous porphyrin ring, which binds iron in such proteins as hemoglobin,[1] myoglobin,[1] peroxidases,[2] and cytochromes,[3] the Co corrin ring of coenzyme B_{12},[4] the corphin ring of methylreductase F_{430} from methanogenic bacteria, which binds nickel,[5] the iron isobacteriochlorin ring of sulfite reductase siroheme,[6] and the di-β-oxoporphyrin ring[7] of dissimilatory nitrite reductase heme d_1, which binds iron.[8] The corphin and corrin rings of methylreductase F_{430} and coenzyme B_{12}, respectively, appear to have been chosen for their flexibility, which modulates Co-C bond cleavage in coenzyme B_{12}[9] and axial ligation[10] and possibly redox properties[11] of the Ni center in methylreductase F_{430}. Crystal structures of the enzymes have shown that the corrin[12] and corphin[13] rings are considerably more ruffled than the porphyrin rings in hemoglobin and myoglobin, for example.[14] This trend has also been demonstrated with nonprotein bound corphins[10b] and porphyrins.[15]

We are interested in understanding the role that the di-β-oxoporphyrin-II ring (structure **4** in Figure 1)[8] plays in the chemistry of dissimilatory nitrite reductase heme d_1. The enzyme functions in a redox capacity accepting reducing equivalents from donor c-type cytochromes and transfers these to nitrite, reducing it to nitric oxide. It consists of a dimer whose subunits each contain two hemes, one type c and the other type d_1.[16]

Although di-β-oxoporphyrin ring oxidation potentials are similar to those of porphyrins[17,18] their $Fe^{3+/2+}$ potentials are approximately 0.25 V more positive than those of porphyrins.[17] In contrast, $Fe^{3+/2+}$ potentials vary by less than 0.10 V from iron isobacteriochlorin and iron chlorin to iron porphyrin.[19] These data indicate that the di-β-oxoporphyrin ring modulates bound

* To whom correspondence should be addressed.

(1) Ten Eyck, L. F. In *The Porphyrins*; Dolphin, D., Ed.; Academic Press: New York, 1979; Vol. VII, Chapter 10.
(2) Hewson, W. D.; Hager, L. P. In *The Porphyrins*; Dolphin, D., Ed.; Academic Press: New York, 1979; Vol. VII, Chapter 6.
(3) (a) Ortiz de Montellano, P. R. *Acc. Chem. Res.* **1987**, *20*, 289-294. (b) Wilson, D. F.; Erecinska, M. In *The Porphyrins*; Dolphin, D., Ed.; Academic Press: New York, 1979; Vol. VII, Chapter 1. (c) Cramer, W. A.; Whitmarsh, J.; Horton, P. In *The Porphyrins*; Dolphin, D., Ed.; Academic Press: New York, 1979; Vol. VII, Chapter 2. (d) Timkovich, R. S. In *The Porphyrins*; Dolphin, D., Ed.; Academic Press: New York, 1979; Vol. VII, Chapter 5.
(4) Golding, B. T. In B_{12}; Dolphin, D., Ed.; Wiley: New York, 1982; Vol. 1, Chapter 15.
(5) Pfaltz, A. In *The Bioinorganic Chemistry of Nickel*; Lancaster, J. R., Ed.; VCH Publishers: New York, 1988; Chapter 12.
(6) Siegel, L. M. *Dev. Biochem.* **1978**, *1*, 201-214.
(7) Abbreviations and numbering scheme are as follows: NiMP (nickel mono-β-oxoporphyrin, **2b**), [3,3,7,8,12,13,17,18-octaethyl-2(3*H*)-porphinonato(2-)] nickel; NiDP-I (nickel di-β-oxoporphyrin-I, **3b**), [3,3,7,8,12,13,17,17-octaethyl-2,18(3*H*,17*H*)-porphinedionato(2-) nickel; NiDP-II (nickel di-β-oxoporphyrin-II, **4b**), [3,3,8,8,12,13,17,18-octaethyl-2,7(3*H*,8*H*)-porphinedionato(2-) nickel; NiDP-III (nickel di-β-oxoporphyrin-III, **5b**), [3,3,7,7,12,13,17,18-octaethyl-2,8(3*H*,7*H*)-porphinedionato(2-) nickel; NiDP-IV (nickel di-β-oxoporphyrin-IV, **6b**), [3,3,7,8,12,12,17,18-octaethyl-2,13-(3*H*,12*H*)-porphinedionato(2-) nickel; NiDP-V (nickel di-β-oxoporphyrin-V, **7b**), [3,3,7,8,13,13,17,18-octaethyl-2,12(3*H*,13*H*)-porphinedionato(2-) nickel; NiTP-A (nickel tri-β-oxoporphyrin-A, **8b**), [3,3,7,8,12,12,18,18-octaethyl-2,13,17(3*H*,12*H*,18*H*)-porphinetrionato-(2-) nickel; NiTP-B (nickel tri-β-oxoporphyrin-B, **9b**), [3,3,8,8,13,13,17,18-octaethyl-2,7,12(3*H*,8*H*,13*H*)-porphinetrionato(2-) nickel.
(8) Chang, C. K. *J. Biol. Chem.* **1985**, *260*, 9520-9522.
(9) (a) Geno, M. K.; Halpern, J. *J. Am. Chem. Soc.* **1987**, *109*, 1238-1240. (b) Babior, B. M. In B_{12}; Dolphin, D., Ed.; Wiley: New York, 1982; Vol. 2, Chapter 10.

0020-1669/91/1330-4654$02.50/0